A Fractographic Investigation of Thermal Embrittlement in Cast Duplex Stainless Steel

T. KOBAYASHI and D. A. SHOCKEY

The fracture surface topography analysis (FRASTA) technique under development at SRI was applied to seek an explanation for severe thermal embrittlement observed in cast duplex stainless steel. By comparing topographic features of conjugate fracture surfaces, FRASTA showed that fracture in thermally embrittled cast duplex stainless steel occurs by microcrack initiation at delta-phase grain boundaries and at alpha-phase/gamma-phase interfaces, and by microcrack growth along these boundaries and interfaces. The critical crack tip opening displacement (CTOD) as measured from cross-sectional views generated by the FRASTA technique indicated a microcrack initiation toughness, J_{Ic}, of 287 KJ/m^2, in excellent agreement with measurements using conventional fracture mechanics procedures, and significantly less than the toughness of unaged material.

I. INTRODUCTION

DUPLEX stainless steels are Fe-Cr-Ni alloys that have a microstructure consisting of two primary phases: austenite (gamma) and ferrite (alpha). Metallurgical overviews of duplex stainless steels are provided in the articles by Solomon and Devine.[1,2] These steels are of particular interest to the nuclear industry because they exhibit high strength and fracture toughness, high resistance to pitting and crevice corrosion, and less susceptibility to sensitization and intergranular corrosion than austenitic stainless steel. However, the use of duplex stainless steels by utilities is as yet negligible because of concerns related to thermal embrittlement, that is, the long-term performance when the materials are subjected to temperatures as low as 250 °C for an extended period.

Thermal-embrittlement characteristics of duplex stainless steels have been investigated by many researchers.[2–8] The well-recognized 475 °C embrittlement is associated with the separation of the ferrite into an iron-rich alpha phase and a chromium-rich alpha-prime phase (the lowest-temperature decomposition product of ferrite in a duplex stainless steel).[1,2,4,5] The concern is that this precipitation of the alpha prime that gives rise to the phenomenon of 475 °C embrittlement may also degrade the toughness after long exposures to temperatures as low as 250 °C,[1,6] making duplex stainless steels unreliable for certain nuclear power applications.

Because of a lack of appropriate experimental data, the embrittlement behavior at low temperatures has been extrapolated from higher-temperature results. Grobner[4] and Solomon[1] found that an Arrhenius rate equation with the Cr diffusion activation energy (48 kcal/mol) could be used to describe low-temperature (475 °C) embrittlement; however, Trautwein and Gysel[6] noted that an activation energy of only 24 kcal/mol would correlate their embrittlement data in the temperature range of 300 to 400 °C for cast duplex stainless steels and that the rate of embrittlement was 10 times faster than that assumed up to now. It is apparent that significant questions still exist regarding the nature and kinetics of the embrittlement mechanisms of alpha prime.

To investigate the thermal embrittlement characteristics of cast duplex stainless steel, the mechanical properties (specifically, the fracture toughness) of a specified alloy in both the as-cast and aged conditions were characterized.[9] The specific aging treatment was 312 hours at 400 °C, which was assumed equivalent to 1.7 years at the nuclear-component operating temperature of 280 °C. The test results indicated that the as-cast material possessed a high fracture toughness [J_{Ic} = 2.49 MJ/m^2 (14,200 in-lb/in^2)], but the fracture toughness of aged material was significantly lower [0.289 MJ/m^2 (1650 in-lb/in^2)], as shown by the fracture toughness-resistance (J-R) curves in Figure 1.[9] (The blunting lines indicated in the figure are computed according to the ASTM standard test method[10] and show crack tip behavior before crack extension.) To seek reasons for this drastic drop in toughness, the microstructures of the two materials were characterized and Charpy impact energies were measured. The results, however, did not provide an explanation.

This paper describes an attempt to delineate important changes in the fracture mechanism due to thermal embrittlement, by quantifying the topologies of the fracture surfaces of an aged specimen and reconstructing the fracture process by computer matching of conjugate fracture surface topographs. This technique, called FRASTA, is described in the next section; the results from applying FRASTA to thermally embrittled cast duplex stainless steel and the conclusions concerning the fracture mechanism, toughness, and

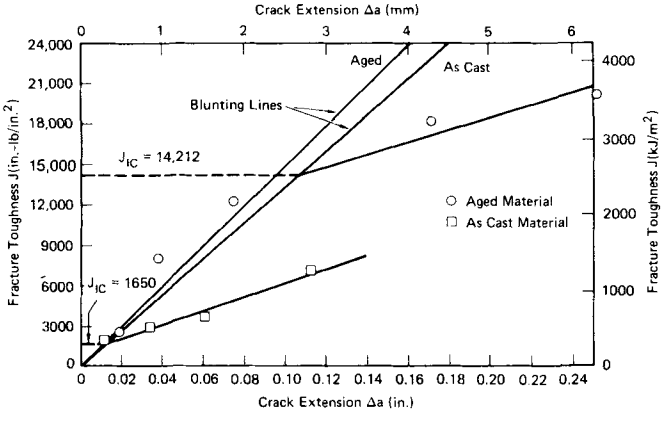

Fig. 1 — Static J-R curve for cast and aged duplex stainless steel.

T. KOBAYASHI, formerly with SRI International, Menlo Park, CA, is with the Department of Mechanical Engineering, Nagoya Institute of Technology, Gokiso-cho, Showa-ku, Nagoya, Japan 466. D. A. SHOCKEY is Director, Department of Metallurgy and Fracture Mechanics, SRI International, Menlo Park, CA 94025.

Manuscript submitted July 22, 1986.

the influences of microstructure are presented in the subsequent sections.

II. FRACTURE EVENT RECONSTRUCTION VIA THE FRASTA TECHNIQUE

The fracture surface topography analysis (FRASTA) technique is a procedure for reconstructing the process of crack extension in microscopic detail by comparing topographic features of conjugate areas of opposing fracture surfaces.[11,12,13] The technique can be used to establish the failure mechanism, *i.e.*, the sequence of microfailure events that occurs in the vicinity of the main crack front as the crack advances through the material. FRASTA also provides continuous measures of local fracture toughness in the forms of crack opening displacement and crack opening angle. Furthermore, the technique, coupled with fractographic and metallographic information, indicates the role of microstructure in the failure process.

To understand how the FRASTA technique can provide details of the fracture mechanism and values for the fracture toughness, one must consider how material fails. Under application of a load, a material generally undergoes local plastic flow before failure begins at some weak spot or stress concentrator in the form of a microvoid or microcrack. The stresses beneath the newly formed microfracture surfaces fall to zero, and the material there relaxes and undergoes no further plastic deformation. The applied load is redistributed to nearby unbroken material, which continues to deform plastically until it fractures. Thus, each increment of microcrack activity is preceded by an increment of plastic flow, a fact that is basic to the FRASTA technique.

As the applied load continues to rise and as the local stresses around the microcrack are transferred to unbroken material, additional plastic flow occurs and other microcracks and microvoids initiate, grow, and eventually coalesce. Each initiation event and each growth increment is accompanied by local deformation, and the deformed material is left in relief on the developing fracture surface. Thus, each tiny volume of material involved in the separation process first deforms, then stops deforming when it fails, while adjacent unbroken material continues to deform until it, too, fails. This sequential deformation and failure process produces irregularities on the fracture surface, and hence the sequence of microfracturing is recorded in the topography of the fracture surface. The local incremental deformation of the fracture surfaces allows the sequence of microfracturing to be determined and the macrofracture event to be reconstructed; this procedure is the basis of the FRASTA technique.

To access the information recorded as roughness on the fracture surfaces, we determine quantitatively the topography of the surfaces by photographing the surfaces in stereo with a scanning electron microscope. Accurate stereopairs are produced by aligning the fracture surface normal to the axis of the microscope and then rotating the stage 4 deg to the left and to the right, taking photographs at each orientation.

The semiautomated cartographic equipment of an aerial surveying company is used to extract the topographic information from the stereo fractographs. These data are digitized and compiled in a computer and are displayed as topographic maps. The failure process can be analyzed at any desired level of detail by analyzing stereo fractographs of appropriate magnification.

In preparation for reconstructing the fracture process, the topographic map of one fracture surface is inverted and superimposed on the map of the conjugate surface. The two maps then are translated and rotated with respect to each other until identifiable corresponding points on the two surfaces are in alignment. Then the relative distance between the maps is adjusted so that the topographic surfaces overlap everywhere; that is, no spaces exist between them.

The fracture process is reconstructed by increasing the distance between the conjugate maps in small increments. After each displacement the projected area is scanned to determine whether overlap is still complete or nonoverlapping regions appear. Gaps between the conjugate maps signify material separation. Gap location and size indicate the location and size of a microcrack. Increase in gap size with successive map displacement indicates microcrack growth behavior, and merging of adjacent gaps illustrates microcrack coalescence behavior. The gradual shrinkage of overlap areas between converging gaps corresponds to the narrowing and stretching of ligaments of material connecting the separating fracture surfaces. These results can be displayed as fractured-area projection plots, as cross sections through the cracking material, and as three-dimensional gap profiles.

FRASTA, at its present stage of development, does not consider possible history effects during formation of the fracture surface. Once a microseparation appears, that area of free surface is assumed to be unaffected by subsequent deformation and separation in adjacent material. Further, the technique considers only the component of deformation perpendicular to the macrofailure surface. Deformation parallel to the fracture surface, although much smaller, may also exist, and could change the topography of existing microfailure surfaces. It is difficult to estimate how much the history effect and lateral deformation influence the final surface topography. The magnitude of the effects may vary with material and loading conditions. However, our experience with FRASTA suggests the effects are small. In each of the fracture problems treated thus far,[11-15] close matching of conjugate topographs was achieved even near to complete overlap.

III. DETERMINATION OF THE FRACTURE MECHANISMS

The fracture surface topographic investigation was carried out on a 1-inch-thick compact tension specimen of a cast duplex stainless steel aged at 400 °C for 312 hours and tested and characterized by Fracture Control Corporation.[9] After fatigue precracking, the specimen was monotonically loaded at a rate of 4.4 MPa-$m^{1/2}$/s (4 ksi-$in^{1/2}$/s) at 21 °C. The loading was interrupted after the crack extended 1.52 mm (average extension through the thickness). The crack extension was marked by heat-tinting; then the specimen was fractured in two by pulling it apart at low temperature.

The fracture resistance curves during crack extension for the as-cast and thermally embrittled material are shown in Figure 1.[9] The tensile properties are tabulated in Table I.[9]

Table I. Tensile Properties of Duplex Stainless Steel[9]

	Yield Strength σ_y (MPa)	Tensile Strength σ_u (MPa)	Flow Stress σ_0 (MPa)*	Elongation (Pct)	Reduction in Area RA (Pct)	Hardness (R_b)
As-Cast						
22 °C	325.4	577.8	451.6	51	61	85
300 °C	203.4	432.3	317.9	30	66	—
Aged						
22 °C	366.8	516.4	442.0	51	40	90
300 °C	227.5	468.9	348.2	28	62	—

*$\sigma_0 = \frac{1}{2}(\sigma_y + \sigma_u)$

Detailed examination of the fracture surface revealed the existence of a significant number of non-heat-tinted islands (unbroken ligaments) in the heat-tinted region. We also observed that the fatigue precrack and heat-tint fronts were irregular. Furthermore, the amount of stable crack extension varied from approximately 3 mm in the center region to about 0.1 mm near the outer edges. Figure 2 shows the highlighted locations of the fatigue precrack front, unbroken ligaments, and the front of the heat-tinted area.

Figure 3 shows the corresponding topographic maps of conjugate areas of the fracture surfaces in the center of

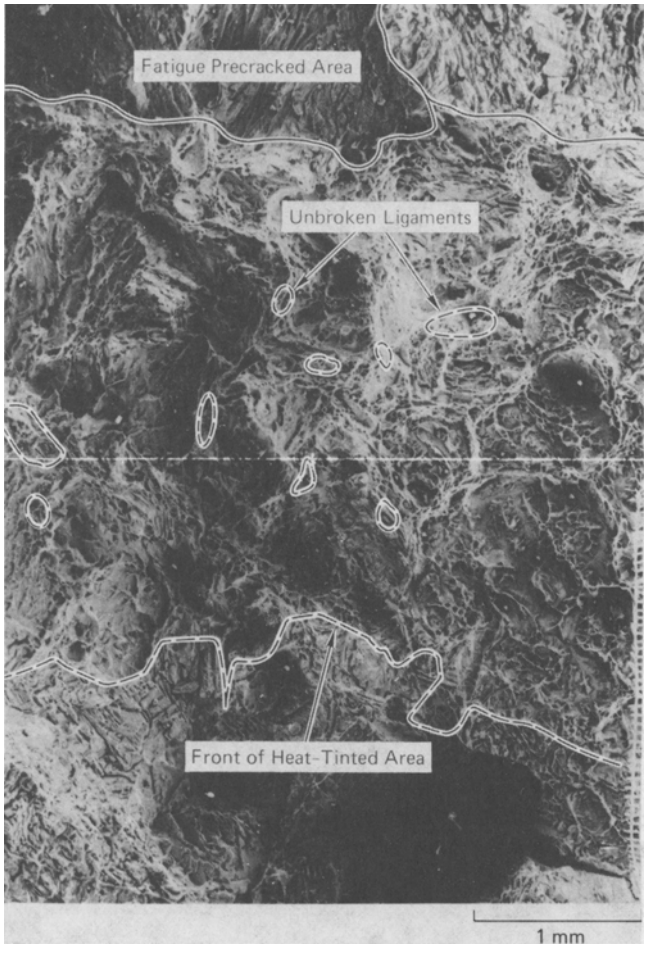

Fig. 2 — Scanning electron micrograph of the fracture surface of cast and aged duplex stainless steel.

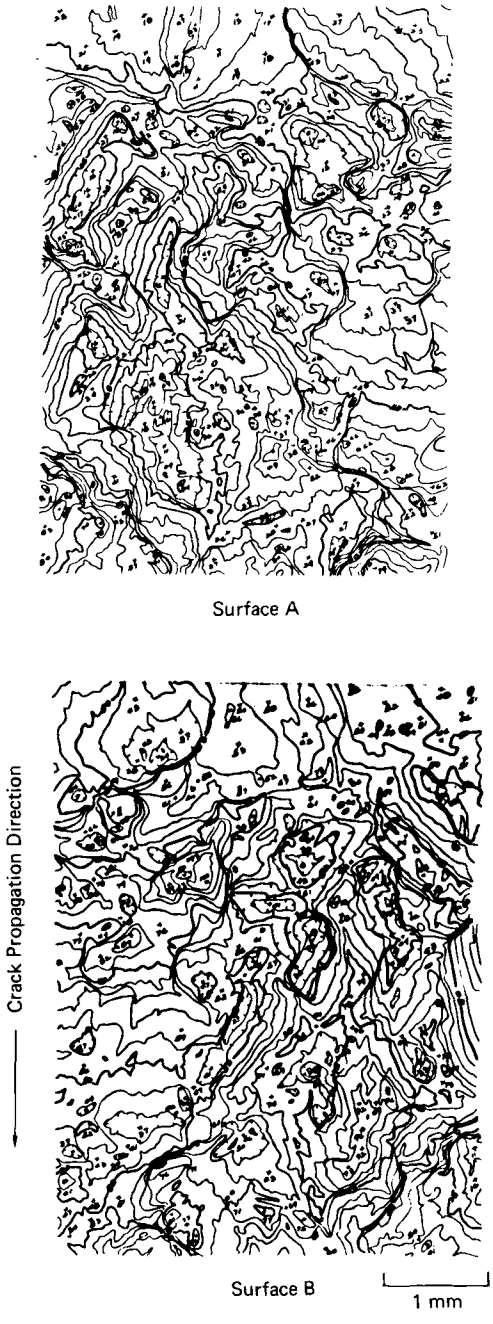

Fig. 3 — Topographic maps of conjugate fracture surface areas in the specimen center.

the specimen. The crack propagation direction is from top to bottom. The fracture surface elevation shown in the topographic maps was measured from an arbitrary reference plane.

Figure 4 shows a series of fractured-area projection plots obtained by incrementally separating the conjugate topographic maps in steps of 32 to 64 μm. In these plots the dark areas indicate continuous material, and white areas are the fractured areas. The numbers found at the upper right indicate the separation between the arbitrarily selected reference planes of the conjugate maps in microns. The difference between any pair of numbers indicates the amount of incremental separation. The orientation of the view shown in Figure 4 corresponds to the SEM fracture surface photograph in Figure 2 and the topographic map for Surface A in Figure 3.

Initially, the conjugate topographic maps were matched by maintaining their reference planes parallel; however, the fracture features that emerged (*i.e.*, fatigue precrack front and heat-tinted area front) did not agree with the actual features observed on the fracture surface. We then tilted one map with respect to the other before matching the conjugate maps so that a larger separation was observed behind the crack tip. We found that a specific tilt angle produced the best agreement in the shape of the fatigue precrack front, locations of unbroken ligaments, and the shape of the heat tint front. We are speculating that this tilt angle may correspond to the continuum crack tip opening angle used to characterize the fracture resistance of steels.[16] Later in this paper we will measure the crack tip opening displacement, δ, resulting from this matching constraint and compare it to the J_{Ic} value that was determined by conventional methods.

Figure 4(a) illustrates the specimen state at the onset of monotonic loading. The fatigue precrack front indicated by the computational conjugate contour matching agrees well with the actual fatigue precrack front observed in Figure 2.

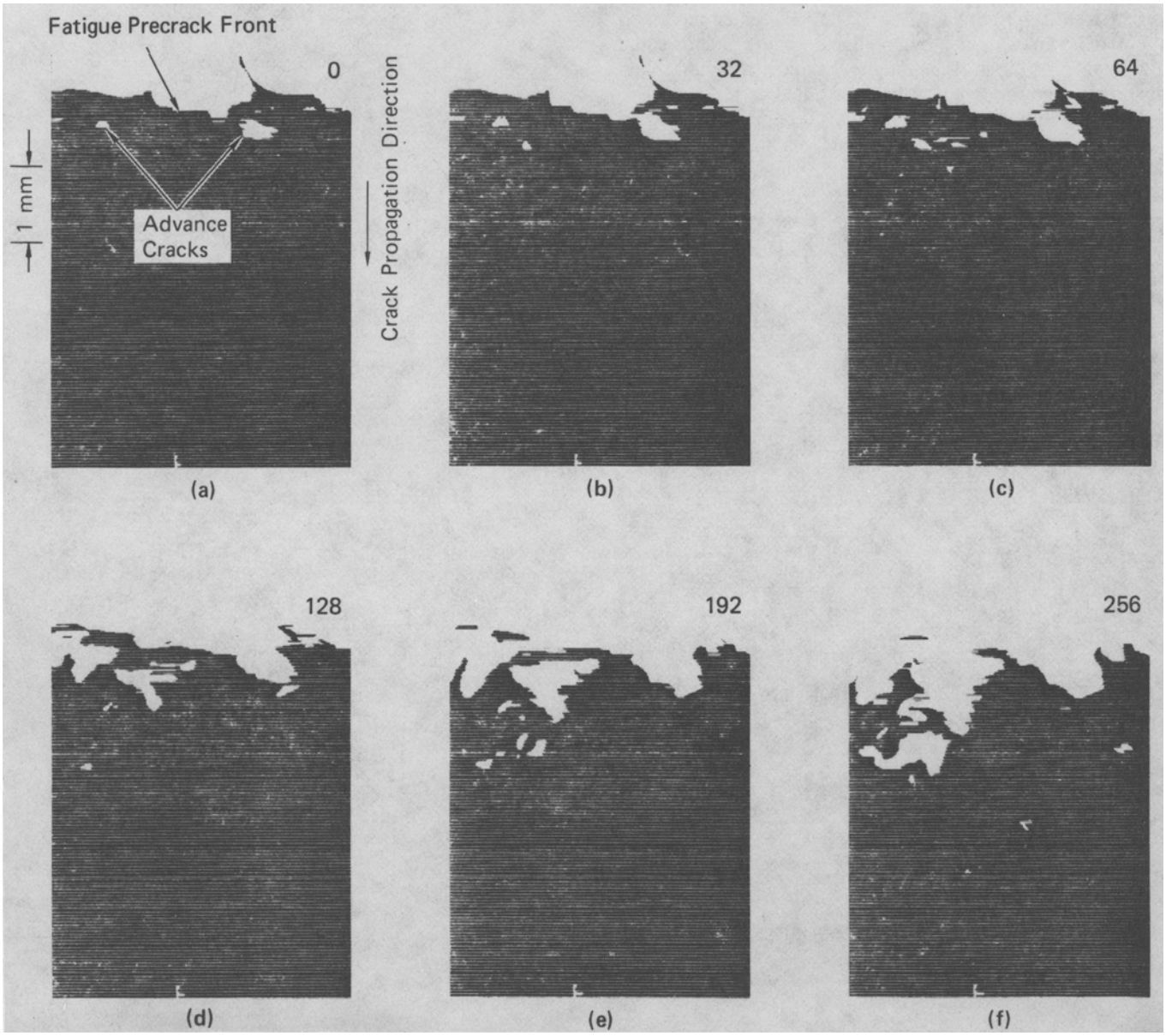

Fig. 4—Fractured-area projection plots showing sequence of fracturing

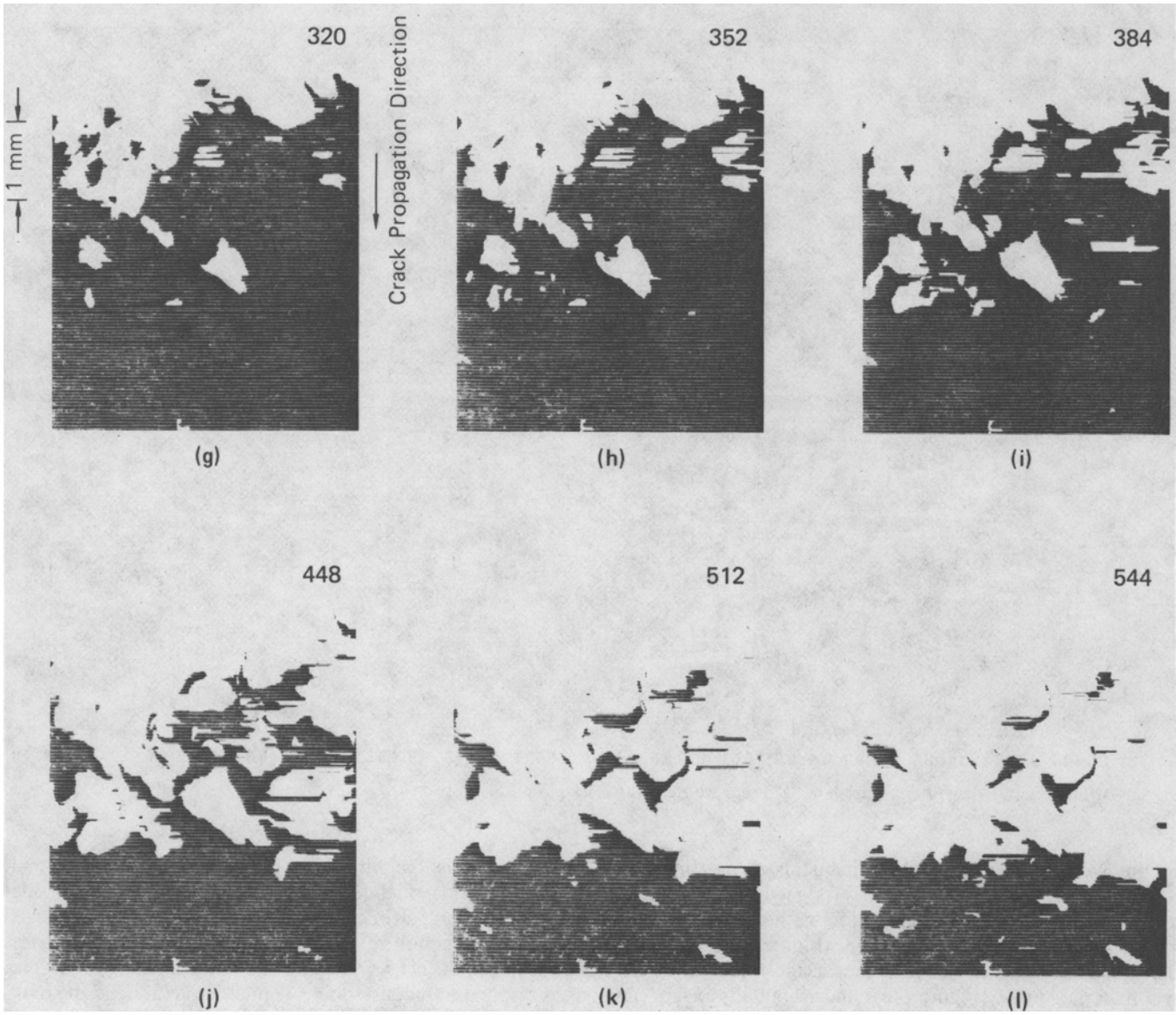

Fig. 4 Cont. — Fractured-area projection plots showing sequence of fracturing.

Figure 4(a) also shows microcracks ahead of the fatigue precrack front, possibly formed during fatigue cycles. Distinct features associated with crack extension are revealed in Figure 4. As the separation between the conjugate maps increased (this is equivalent to increased load on the specimen or increased deformation of the specimen), the existing microcracks increased in size and coalesced with the main crack front [Figure 4(b)]. Also, new microcracks were formed, grew, and merged with each other to form larger microcracks before coalescing with the main crack front [Figures 4(c) through 4(f)].

It is important to note that, during the sequence between Figures 4(c) through 4(f), although the maps were separated with 64-μm increments, the main crack front did not advance appreciably; however, an examination of Figures 4(g) through 4(i) reveals rapid acceleration in microcrack formation and growth and in the main crack front movement despite a reduced separation increment of 32 μm. We interpret this accelerated failure activity as the onset of crack growth, which begins in Figure 4(g).

Figures 4(b) through 4(j) clearly demonstrate that the mechanism of crack extension in this material can be described as nucleation, growth, and coalescence of microcracks with the main crack front. This mechanism produces an irregular crack front and results in the formation of unbroken ligaments, as shown in Figures 4(j) through 4(l).

Figure 4(l) corresponds to the state at which the fracture test was interrupted. The locations of the predicted main crack front and unbroken ligaments agree well with those shown in Figure 2.

Figure 5 shows cross-sectional views of crack growth obtained by displacing topographic contours along a center plane normal to the fracture surfaces. (The darkly-shaded areas are areas where the two topographic surfaces overlap.) It was not determined whether the profile shown in Figure 5(a) represented the configuration of the crack before or shortly after monotonic loading began. Figures 5(a) through 5(c) illustrate clearly significant crack tip blunting during the initial phase of the monotonic loading. At Figure 5(c), the main crack front is about to extend by

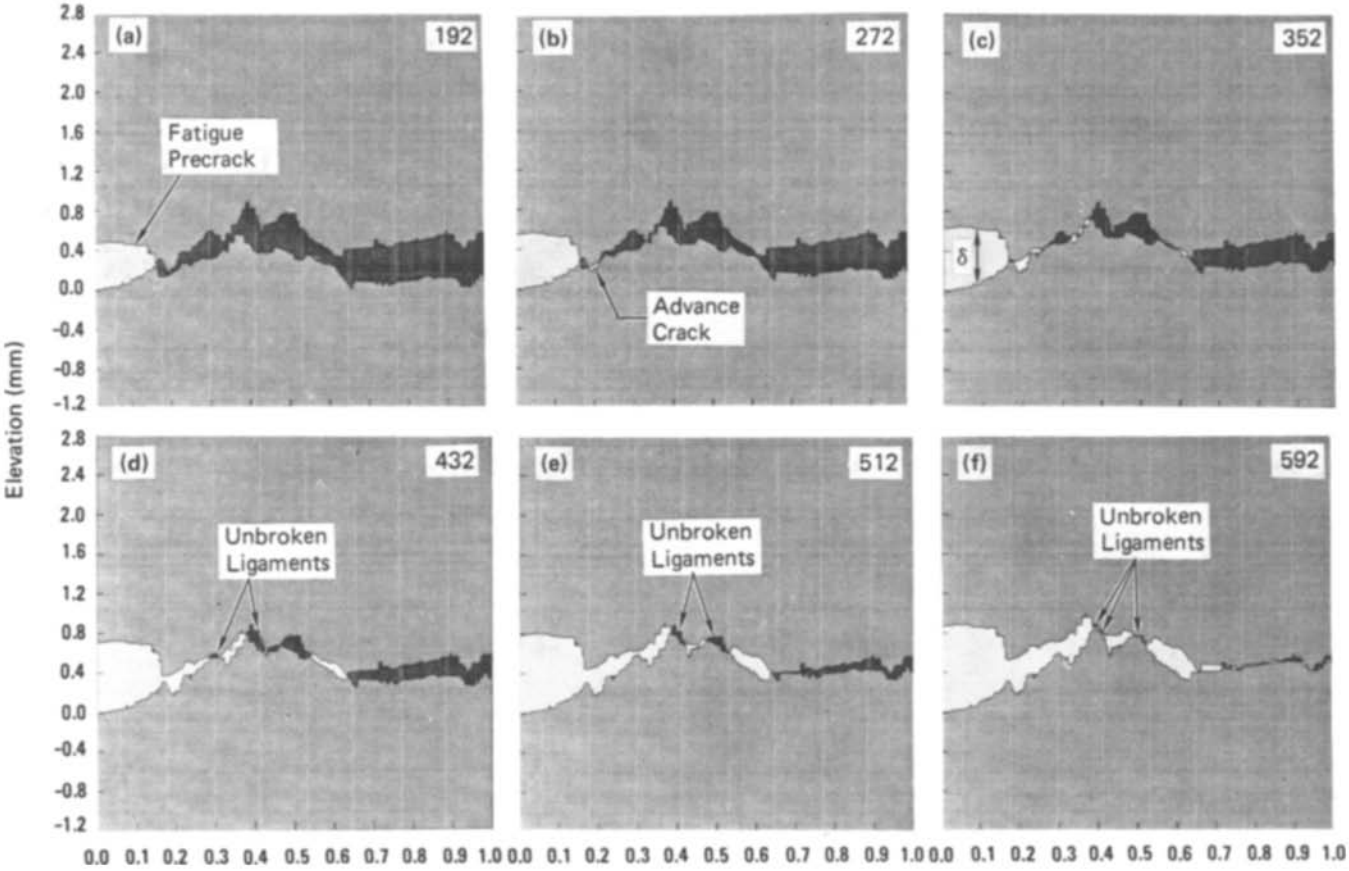

Fig. 5—Cross-sectional view of crack tip showing successive stages of crack propagation.

joining with the advance cracks. Ligaments of material connecting the fracture surfaces are produced as the microcracks ahead of the main crack tip join with one another and isolate islands of unbroken material [Figure 5(d)]. On further loading (additional displacement), these islands of intact material shrink [Figure 5(e)] and eventually disappear [Figure 5(f)] as the microcracks continue to grow and sever the ligaments.

The crack tip opening displacement (CTOD) observed at the tip of the fatigue precrack in Figure 5(c)—that is, at the onset of crack extension—is 0.65 mm. We used this value to compute crack initiation toughness, J_{Ic}, by taking the flow stress σ_0 to be 442 MPa (see Table I) and multiplying σ_0 and the CTOD. The resulting value, $J_{Ic} = 287$ KJ/m^2, agrees well with the J_{Ic} value of 284 KJ/m^2 obtained using a conventional fracture test procedure.[9]

IV. RELATING FRACTURE SURFACE FEATURES TO MICROSTRUCTURE

The sites of microcrack initiation indicated by the fractured-area projection plots in Figure 4 were compared with the fracture surface photograph in an attempt to identify the microstructural features responsible for microcrack initiation. The results are shown in Figure 6. The arrows labeled A point to several large, slanted planes on the topographs; the arrows labeled B point to layered or laminate structure. Unlabeled arrows indicate initiation sites at which distinguishing features could not be observed.

To establish relationships between microstructure and fracture surface features, the specimen was sectioned along the white vertical line shown in Figure 6. Figure 7 shows the microstructure revealed by an electrolytic (5 VDC for 5 seconds) 40 pct KOH etch. The white areas in the figure correspond to an austenitic (gamma) structure and the dark areas to a ferritic (alpha) structure. Furthermore, we observed that this material exhibits a macrostructure and that the macrograin (delta-grain) boundaries influence the crack path significantly. For example, at the leading edge of the stable crack growth region in Figure 7(a), the crack path was parallel to the macrograin boundary. In the region fractured at low temperature after the test, shown in Figure 7(b), the crack also ran along some sections of the macrograin boundaries.

Comparison of the microstructure shown in Figure 7 with the fracture surface features shown in Figure 6 reveals that fine steps and scratchlike features represent deformed gamma-phases; that the large, slanted planes marked by the arrows labeled A are related to the delta-grain boundaries; and that the fracture initiation sites labeled B may be associated with crack initiation between the gamma-phase platelets.

Other interesting features observed in the stable crack growth region are the small cracks formed under the fracture surface and the deformation of the material around them. Figure 8(a) shows a magnified view of one such crack and the area surrounding it. It is apparent that the crack occurred at the interface between the alpha and gamma phases. The crack was arrested on the left side by the long gamma phase;

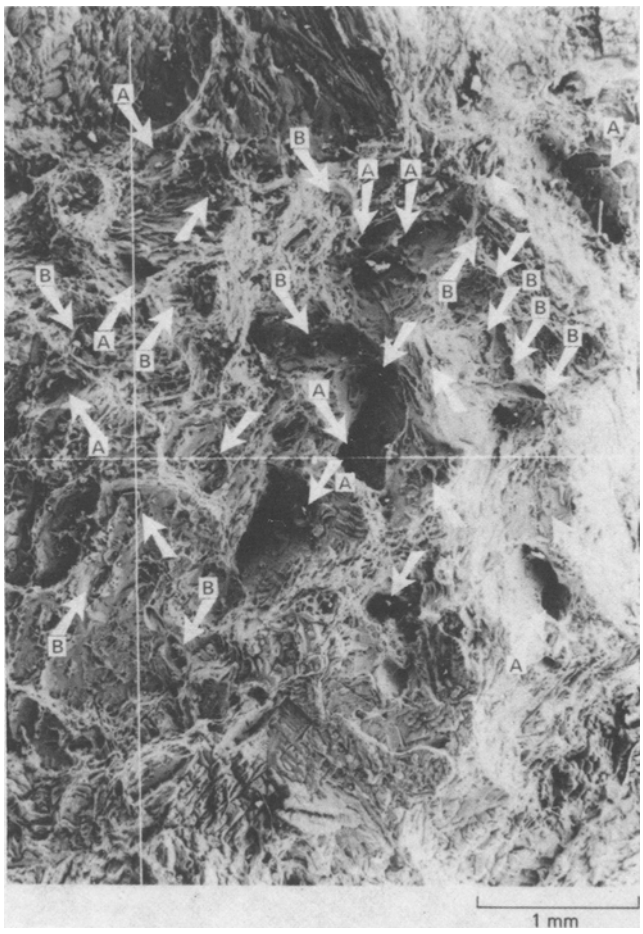

Fig. 6—Microcrack initiation sites on the fracture surface as indicated by FRASTA.

on the right side, however, the crack changed direction and appeared to connect to the main fracture surface. Large plastic deformation in the gamma phase is indicated by the pits produced during etching.

We note in passing that the principle of conjugate topographic-contour matching is demonstrated on the section shown in Figure 8(a). If we cut the picture along the line shown in Figure 8(a) and shift the portion of the picture above the crack downward until the conjugate surfaces of the small crack contact, we can reconstruct the material as it was before the crack formed, as demonstrated in Figure 8(b). Comparison of the width of the long gamma phase in Figures 8(a) and 8(b) indicates that this gamma strip increased its width 50 pct and the plastically deformed parts overlapped when the section of the picture was shifted down [Figure 8(b)].

The results presented here were obtained from SEM fracture surface photographs taken at low magnification; thus, it was not possible to determine whether precipitates or inclusions at the interfaces triggered the microfailure at these sites. Topographic analysis with higher-magnification SEM photographs may be able to resolve these questions. In addition, the microfailure initiation sites determined by the topographic analysis can be further examined using high-magnification scanning microscopy and X-ray energy dispersive spectrum analysis.

V. SUMMARY

The fractured area projection plots generated by FRASTA clearly show that crack propagation in thermally embrittled cast duplex stainless steel occurs by the nucleation, growth, and coalescence of microcracks in material ahead of the main crack tip. Furthermore, the sequence of these microcracking events, the sites of microcrack initiation, and the mode of microcrack growth and coalescence are clearly indicated. By superimposing these plots on the fracture surface photographs, we were able to correlate these microcracking processes with microstructural features and determine that microcracks initiate at and grow along delta-phase grain boundaries and alpha-phase/gamma-phase interfaces. By presenting the results as cross-sectional views, we could determine the crack opening displacement at desired locations along the crack front and use the results to calculate the fracture toughness, as demonstrated by Figure 5.

Thus, in examining the fracture of thermally embrittled cast duplex stainless steel, the FRASTA technique was successful in characterizing the details of macro- and microfracture, in correlating microcracking events with microstructural features, and in providing local measurements of macroscopic fracture toughness. To explain further how thermal aging reduces the fracture resistance of duplex stainless steel, the results from the FRASTA examinations reported here should be compared with FRASTA results on an unaged specimen.

ACKNOWLEDGMENTS

This work was sponsored by Electric Power Research Institute, Palo Alto, CA, under Project No. RP1757-22. The authors would like to thank Drs. Theodore U. Marston, Robin L. Jones, and Douglas M. Norris of EPRI for their interest, technical advice, and encouragement in developing and applying the FRASTA technique. We are grateful to Mr. Jan Terry of SRI for assistance in producing the scanning electron microscope stereophotographs; Mr. James Kemp of SRI for developing computer programs for the topographic data processing, conjugate topographic contour matching, and display of the results; and Mr. Richard A. Cowan of Grenier Aerial Surveys, Inc., Sacramento, CA, for making it possible to produce topographic maps from stereopairs of scanning electron microscope photographs. Finally, we are indebted to Dr. Paul McConnell of Fracture Control Corporation for providing the fractured specimen and test data.

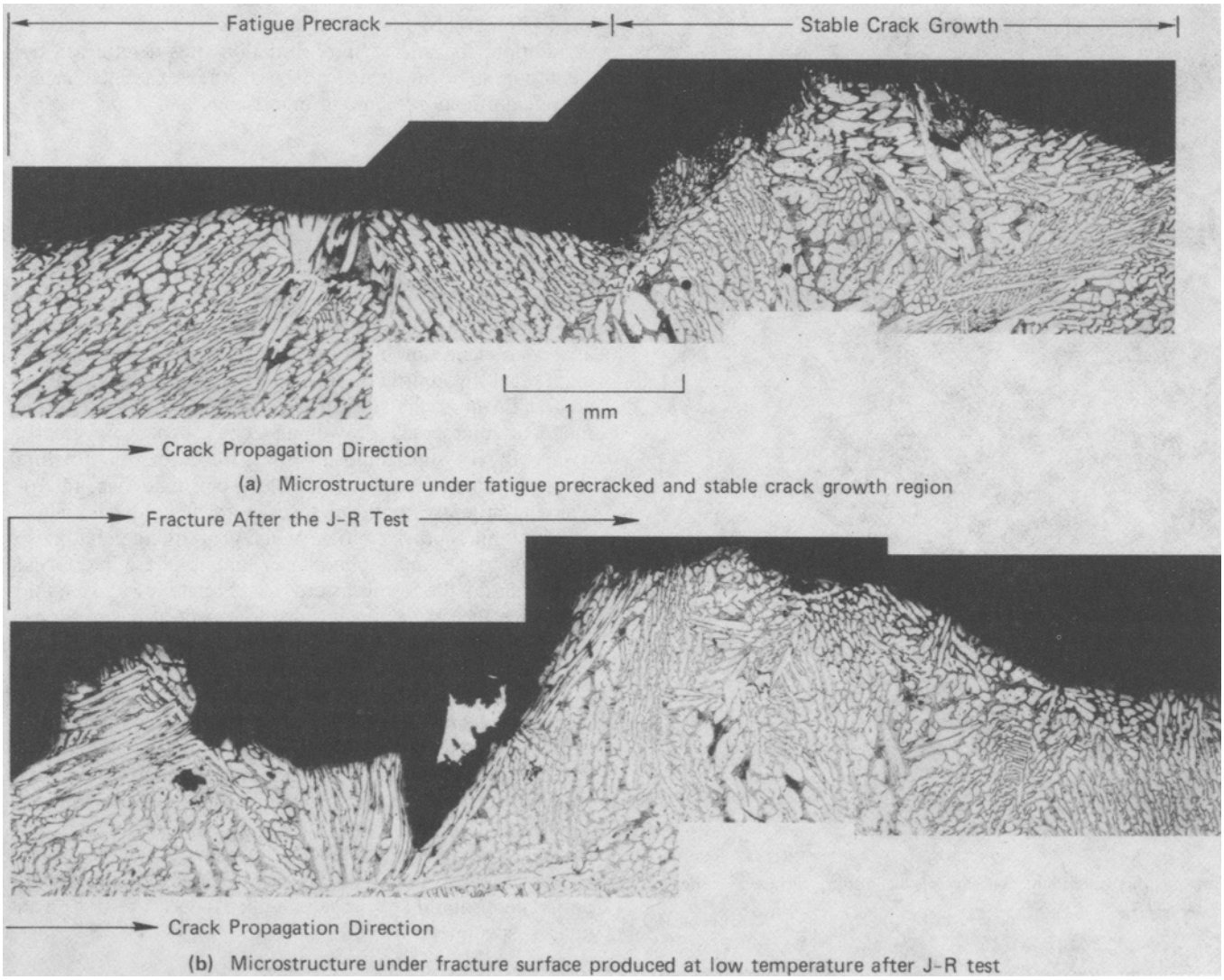

Fig. 7 — Microstructural detail beneath the fracture surface in duplex stainless steel.

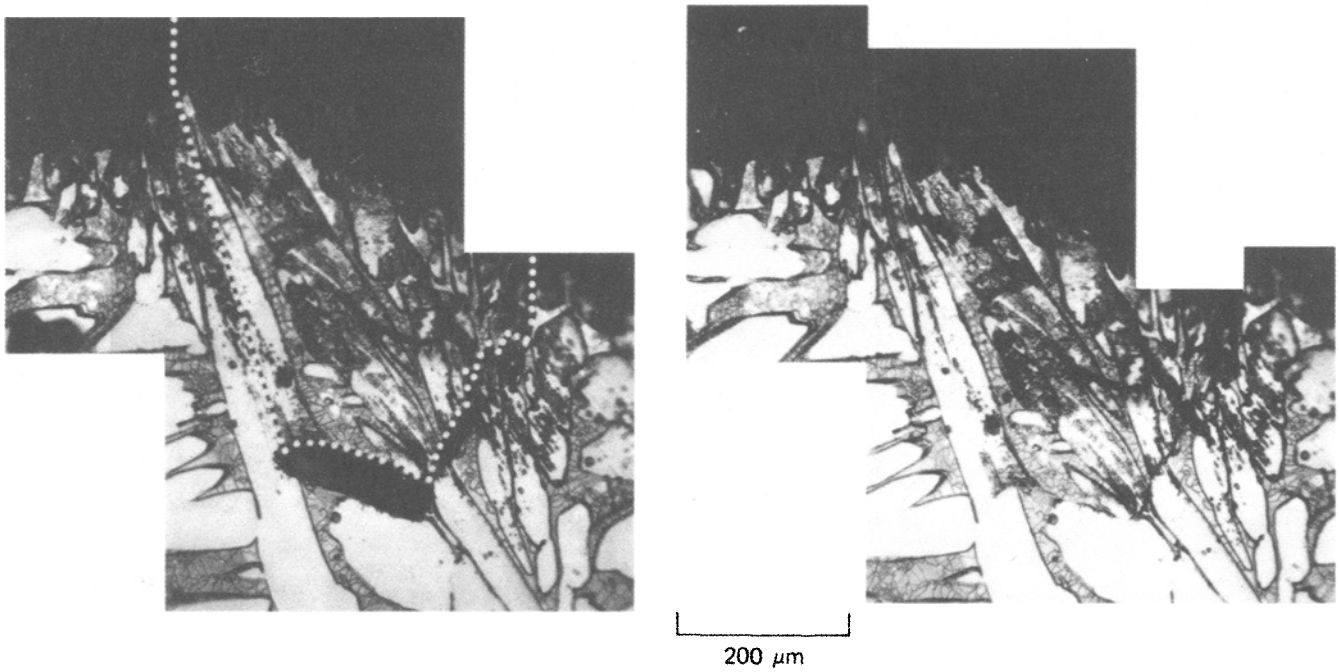

(a) Crack under fracture surface (Dark area-α phase; Light area-γ phase)

(b) Matching of crack surfaces by shifting downward the material above the crack

Fig. 8—Microcrack formation at alpha-phase/gamma-phase interface illustrating the principle of FRASTA.

REFERENCES

1. H. D. Solomon and T. M Devine, Jr.: *Duplex Stainless Steels*, R. A. Lula, ed., ASM, Metals Park, OH, 1983, pp. 693-756.
2. H. D. Solomon and T. M. Devine, Jr.. *MiCon 78: Optimization of Processing, Properties, and Service Performance Through Microstructural Control*, ASTM STP 672, Halle Abrams, G. N. Maniar, D. A Nail, and H. D. Solomon, eds., American Society for Testing and Materials, 1979, pp. 430-61
3. R. O. Williams: *Trans. TMS-AIME*, 1958, vol 212, pp. 497-502.
4. P. J. Grobner: *Metall. Trans.*, 1973, vol. 4, pp 251-60
5. T. J. Nichol, A. Datta, and G. Aggen: *Metall. Trans. A*, 1980, vol 11A, pp. 573-85.
6. A. Trautwein and W. Gysel: *Spectrum*, technical publication of Georg Fisher Company, Schaffhausen, Switzerland, 1981, vol. 5, pp 38-48
7. H D Solomon. *Duplex Stainless Steels*, R. A. Lula, ed., ASM, Metals Park, OH, 1983, pp. 41-69.
8. J. E Truman and K. R. Pirt: *Duplex Stainless Steels*, R A. Lula, ed , ASM, Metals Park, OH, 1983, pp. 113-42.
9. P. McConnell and J. W. Sheckherd· Final Technical Report to the Electric Power Research Institute on Research Project RP1543-2 by Fracture Control Corporation, Goleta, CA, Feb. 1986.
10. Standard Test Method for J_{Ic}, A Measure of Fracture Toughness, E813-81, *1983 Annual Book of ASTM Standards*, vol 03.01, *Metals-Mechanical Testing, Elevated and Low Temperature Tests*, American Society for Testing and Materials, Philadelphia, PA, 1983, p. 762.
11. T. Kobayashi, G. R. Irwin, and E. J. Zhang: *Fractography of Ceramic and Metal Failures*, ASTM STP 827, J. J. Mecholsky, Jr. and S. R. Powell, Jr , eds , American Society for Testing and Materials, Philadelphia, PA, 1984, pp. 234-51.
12. K Ogawa, X. J. Zhang, T. Kobayashi, R. W. Armstrong, and G. Irwin: *Fracture Mechanics: Fifteenth Symposium*, ASTM STP 833, R. J. Sanford, ed , American Society for Testing and Materials, Philadelphia, PA, 1984, pp. 393-411.
13. T. Kobayashi and D. A. Shockey: *Fracture: Interaction of Microstructures, Mechanisms, and Mechanics*, J. W. Wells and J. D. Landes, eds., TMS-AIME, 1984, pp. 447-61.
14. T. Kobayashi and D. A Shockey: Final Technical Report to the Electric Power Research Institute on Research Project RP1757-22 by SRI International, Menlo Park, CA, March 1986.
15. T. Kobayashi and J H. Giovanola: Special Technical Report to the Electric Power Research Institute on Research Project RP2455-7, by SRI International, Menlo Park, CA, Dec. 1985.
16. C. F. Shih, H G. deLorenzi, and W. R Andrews *Elastic-Plastic Fracture*, ASTM STP 668, J. D. Landes, J A. Begley, and G. A. Clarke, eds., American Society for Testing and Materials, 1979, pp. 65-102.